An Improved Zero-Current-Switching Single-Phase Transformerless PV H6 Inverter with Switching Loss-Free

Hua F. Xiao, *Member, IEEE*, Li Zhang, and Yanqing Li

***Abstract*—In this paper, a switching loss-free (SLF) concept for the first six-switches H-bridge inverter (H6-I) topology is proposed. SLF means that its switches are able to operate with soft turn-on and turn-off transitions. In order to implement the SLF goal, a new resonance-trajectory is proposed. Compared with the zero-current-transition H6-I (ZCT-H6-I) topology published in previous literature, the proposed resonance-trajectory can precisely compensate for losses of resonant tanks every switching period. With this intention, an implementing circuit is structured based on the H6-I topology, and its detailed operation principle and performance characteristics are analyzed. As a result, all active switches of the new circuit are switched under zero-current turn-on and zero-current turn-off conditions. Also, the reverse recovery problem of freewheeling diodes is alleviated owing to the zero-current turn-off property of diodes. The SLF target is realized in theory. Finally, experimental results from a 1 kW prototype at 50 kHz switching frequency are provided to verify the effectiveness of the proposed SLF concept in practice. Specifically, the conversion efficiency of the new circuit is over 95% in a wide load range, and there is roughly a 1.5% efficiency improvement compared with the hard-switching H6-I topology.**

***Index Terms*—Zero-current-switching, Resonant tank, switching loss-free, Transformerless PV inverter**

I. Introduction

In recent years, the distributed PV generation system has received an increasing popularity in the residential, commercial, and industrial areas [1-3]. Compared with isolated PV generation configurations, transformerless configurations have become a widespread acceptance due to the attractive efficiency, small volume and low cost [4-10]. Based on these merits, some researchers intend to pursue high power density transformerless PV grid-connected inverters by raising the switching frequency [11-18]. Looking back, this developing trend will resemble the developed route of DC switching supplies in 3C (Computer, Communication and Consumer Electronic) industry, for their switching frequencies have already reached MHz level currently. However, in conventional transformerless PV grid-connected inverters, their switches are still on hard-switching state [4-10]. Because of this, High frequency transformerless PV grid-connected inverters will suffer from high losses, cooling stresses, and EMI noises [11, 12].

Obviously, soft-switching technique is one of the most promising techniques to reduce or even remove the switching losses, and to degrade the switching stresses, such as *di*/*dt* and *dv*/*dt* [19]. Generally speaking, existed soft switching techniques can be roughly categorized into two sorts: the snubber-type with resonant tanks [11, 12, 14, 15, 19-21] and the control-type using switching modulation strategies [13, 22-26]. In previous literature, there were a plenty of snubber-type soft switching topologies resulted from Silicon Controlled Rectifier (SCR) commutating branches [19-21]. Their main aim was at combining desired features from both of the conventional PWM and resonant converters while avoiding their respective disadvantage. Particularly, according to with or without active power devices, the snubber-type soft switching techniques can be further classified as the active snubber-type and passive snubber-type [27, 28]. In active-snubber-types, the resonant tanks can only be activated during switching transitions of high-frequency switches. Therefore, once the switching transition is finished, this kind of converters can revert back to the familiar PWM operation mode so that the circulation loss of resonant tanks can be minimized [11, 12, 29, 30].

Because of the advantages of the active-snubber-type soft switching technique, a ZCT-H6-I transformerless PV grid-connected inverter was proposed in [11]. In its topology, a couple of resonant tanks are added in parallel to the high-frequency main switches around. As a consequence, it realizes the zero-current turn-off for the main switches and zero-current turn-on for their auxiliary switches, respectively. However, there are still two disadvantages in [11]. First, the peak current of the resonant inductors is gradually attenuated in the grid period since the loss of resonant tanks can not be replenished every switching period. Because of this, the ZCT-H6-I may lose the zero-current turn-off condition of the high-frequency main switches in partial ranges. Second, the

Manuscript received October 10, 2016; revised January 01, 2017, February 14, 2017, and March 18, 2017; accepted March 22, 2017. This work was supported in part by the National Natural Science Foundation of China Under Grant 51577033, in part by the Fundamental Research Funds for the Central Universities Under Grant 2242015K1008, in part by the Project of State Grid in China Under Grant SGTYHT/14-JS-188.

The authors are with the College of Electrical Engineering, Southeast University, Nanjing 210096, China (e-mail: xiaohf@seu.edu.cn).

This article has been accepted for publication in a future issue of this journal, but has not been fully edited. Content may change prior to final publication. Citation information: DOI 10.1109/TIE.2017.2694398, IEEE Transactions on Industrial Electronics

turn-off loss of the auxiliary switches and the reverse recovery problem of freewheeling diodes are still retained.

Undoubtedly, there have been two important challenges for the ZCT-H6-I so far. They include compensating for the loss of the resonant tanks every switching period, removing the turn-off loss of the auxiliary switches and the reverse recovery loss of the freewheeling diodes. In order to solve these problems, this paper restructures a resonance-trajectory with a self-compensation mode, as well as a couple of improved resonant tanks with the resonance-trajectory are proposed. Particularly, several distinctive features have been obtained in the proposed circuit: first, the loss of the resonant tanks is reliably replenished by the self-compensation mode every switching period; second, the zero-current-switching (ZCS) conditions of turn-on and turn-off processes are achieved for all power semiconductor devices including diodes. In other words, all switching losses are almost removed, and the reverse recovery problem of the freewheeling diodes is also alleviated because of diode's ZCS turn off. Last and the most important, the SLF concept for transformerless PV grid-connected inverters is successfully realized. These advantages will significantly improve the efficiency of transformerless PV grid-connected inverters, especially in high switching frequency applications.

The major contribution of this paper is to propose and demonstrate a switching loss-free (SLF) concept based on the H6-I topology, which is attractive in high power density transformerless PV grid-connected inverters. This paper is organized as follows. Section II firstly presents the proposed resonance-trajectory with a self-compensation mode, and the improved resonance tanks. After that, this section gains an improved ZCS-H6-I topology with SLF (Hereinafter, the improved circuit is referred as SLF-H6-I). Moreover, the additional operation modes of the SLF-H6-I compared with the ZCT-H6-I are analyzed in this section also. Section III presents the characteristics of the SLF-H6-I, such as soft switching conditions, stresses on power components, thermal losses of semiconductor devices, common-mode performance, as well as non-unity power factor running. Subsequently, some experimental results from a 50 kHz/1 kW SLF-H6-I are provided in Section IV. Finally, a conclusion is given in Section V.

II. Resonant Tank with Self-Compensation Mode

A. State-Plane Trajectory of Resonance Behavior

Before analysis, it is necessary to recall the operation principle of the ZCT-H6-I topology in [11]. Its state-plane trajectory of the resonant tanks is redrawn in Fig. 1(a), and the detailed operation modes can refer to *Section* II. B in [11]. From Fig. 1(a), it can be seen that the circle real line with arrows is the ideal resonance trajectory, which is named as free resonance trajectory. When the loss of the resonant tanks is taken into consideration, the practical resonance trajectory is represented by an asymptotic dash line, which is also shown in Fig. 1(a). Obviously, the peak current of the resonant inductor and the peak voltage of the resonant capacitor are gradually

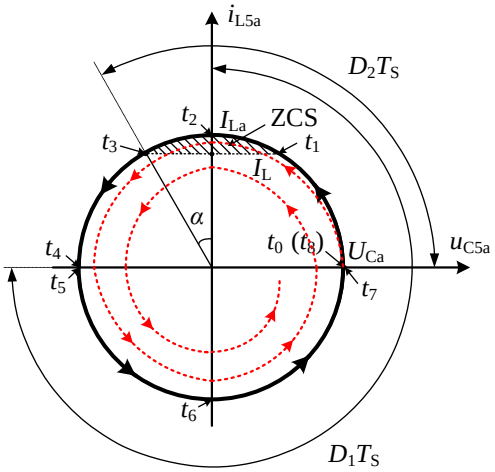

(a)

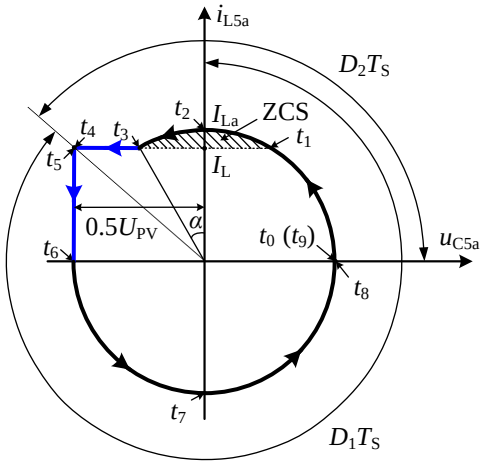

(b)

Fig. 1. State-plane trajectories of different resonant activities (here iL5a and uC5a are the current of the resonant inductor L5a and the voltage of the resonant capacitor C5a, respectively). (a) Ideal and practical trajectories in the ZCT-H6-I [11]. (b) Expected trajectory with a self-compensation mode.

attenuated because the loss of the resonant tanks could not be replenished timely. As a result, the ZCS turn-off condition of the high frequency main switches may not be satisfied in entire operation range.

In order to overcome above disadvantage, an improved resonance trajectory is restructured in this paper, which is shown in Fig. 1(b). It can be seen, a constant current charging period [t_3, t_4] is inserted into the free resonance trajectory at t_3. As a result, this new mode is able to charge the resonant capacitor voltage to the half of the input voltage every resonant period. The new added operation mode is named as self-compensation mode. After this self-compensation mode, a resonant inductor current linear falling period [t_5, t_6] is followed to force the resonant trajectory catch up with the free resonance trajectory at t_3.

B. Implementing Circuit of the Improved Trajectory with Self-Compensation Mode

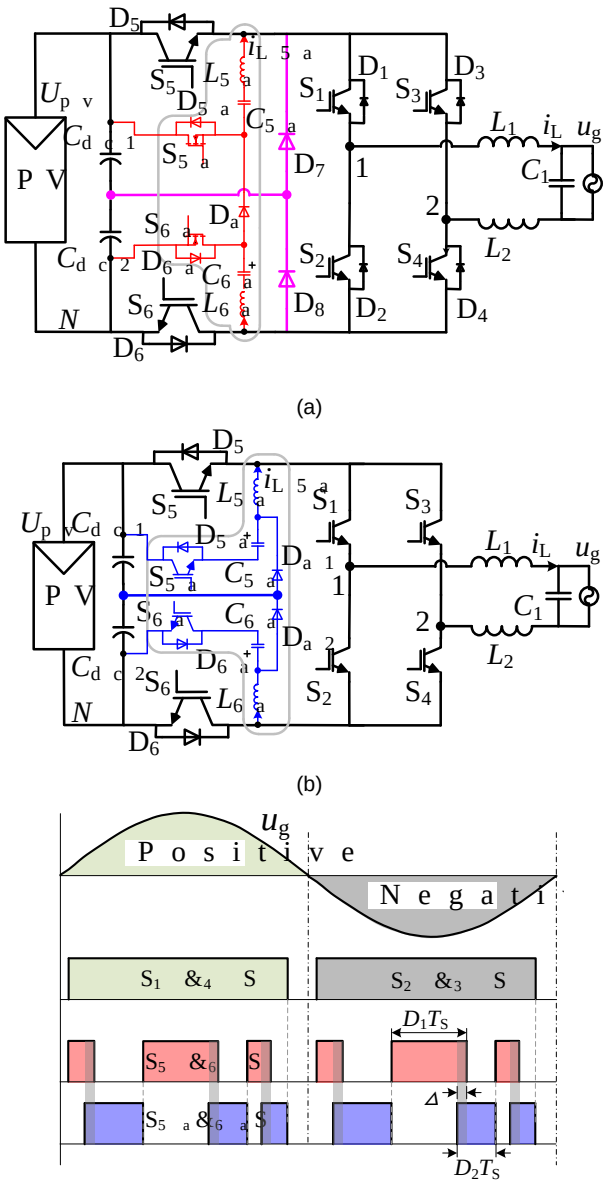

Fig. 2. Topology of [11] and proposed topology with self-compensation mode. (a) ZCT-H6-I [11]. (b) SLF-H6-I. (c) Gate signal sketch of SLF-H6-I (u_g is the grid voltage).

In this section, a pair of improved resonant tanks with the self-compensation mode is derived based on the ZCT-H6-I topology. In detail, the ZCT-H6-I, SLF-H6-I and its driving logic are shown in Fig. 2(a), (b), and (c), respectively. Compared with the previous ZCT-H6-I topology, the connection points of two resonant tanks are moved from the midpoints of the auxiliary switch and resonant capacitor to the midpoints of the resonant capacitor and resonant inductor, respectively. In addition, the previous auxiliary resonant freewheeling branch and common-mode clamping branch are integrated into a freewheeling clamping diode branch composed of D_{a1} and D_{a2}. Especially, the line-frequency switches S_1-S_4 are without anti-parallel diodes. The reason is that the freewheeling current no longer flows through these anti-parallel diodes under the condition of unity power factor.

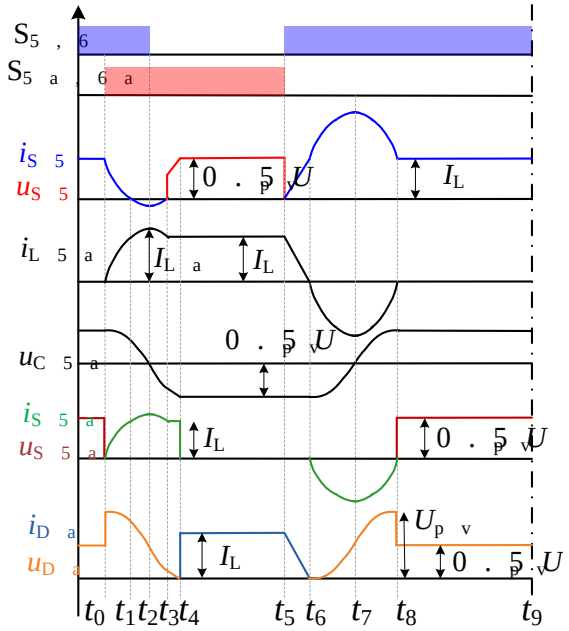

Fig. 3. Key waveforms of the SLF-H6-I in switching frequency scale (u_{S5} and i_{S5} are the collector-emitter voltage and current of IGBT S_5, respectively. u_{S5a} and i_{S5a} are the collector-emitter voltage and current of IGBT S_{5a}, respectively. u_{Da} and i_{Da} are the cathode-anode voltage and current of Diode D_{a1}, respectively.).

The detailed operation analysis and performance for the new circuit are going to be presented in next sections.

On the driving logic hand, the gate signal sketch of all switches is illustrated in Fig. 2(c). As can be seen in Fig. 2(c), the duty cycle of the high frequency main switches S_5 and S_6 is denoted as D_1; the duty cycle of the auxiliary switches S_{5a} and S_{6a} is denoted with D_2. In the positive half cycle of the grid voltage, S_1 and S_4 are always ON, S_2 and S_3 are always OFF. Oppositely, S_1 and S_4 are always OFF, S_2 and S_3 are always ON in the negative half cycle. There is an overlapping time Δ between the high frequency switches (S_5, S_6) and the auxiliary switches (S_{5a}, S_{6a}). These driving requirements are almost the same as at the ZCT-H6-I topology. But their difference is that the previous turn-off constraint condition for the auxiliary switches S_{5a} and S_{6a} of the ZCT-H6-I is relieved in the new resonant tanks.

Referring to Fig. 2(c), the turn on moment of the main switches and the turn off moment of the auxiliary switches can be set freely, such as at the same time point, or with a dead time, or even with an overlapping time. This paper sets the turn on moment of the main switches and the turn off moment of the auxiliary switches at the same time to discuss its operation principle.

C. Operation Principle of the SLF-H6-I Topology

By comparing Fig. 1(b) with Fig. 1 (a), it can be seen that only the operation modes [t_3, t_4], [t_4, t_5], and [t_5, t_6] are new, so they are necessary to analysis in detail. However, the rest of operation modes are not duplicated here since they are similar with the ZCT-H6-I topology in [11]. Therefore, this section focuses on three new operation modes. The key operation waveforms of the SLF-H6-I in the grid current positive half

This article has been accepted for publication in a future issue of this journal, but has not been fully edited. Content may change prior to final publication. Citation information: DOI 10.1109/TIE.2017.2694398, IEEE Transactions on Industrial Electronics

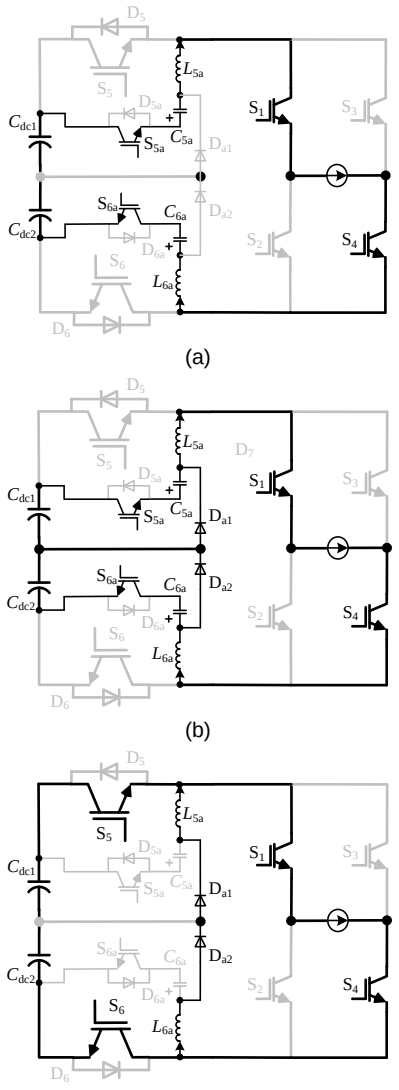

Fig. 4. Equivalent circuits of three new operation modes. (a) Stage 4 [t_3, t_4], (b) Stage 5 [t_4, t_5], (c) Stage 6 [t_5, t_6]

cycle are shown in Fig. 3, and the equivalent circuits of three new operation stages are illustrated in Fig. 4.

1) *Stage 4* [t_3, t_4]: Referring to Fig. 4(a). Upon the fact that the peak value of the resonant currents is larger than the maximum amplitude of the grid current which is guaranteed by designing the resonant parameters [11], the resonant currents i_{L5a} and i_{L6a} fall to I_L at t_3. After that, they are clamped at I_L by the current of the filter inductors L_1 and L_2.

In this period, the resonant inductors and resonant capacitors stop resonating. The resonant capacitors C_{5a} and C_{6a} are charged by the constant current I_L, i.e. the self-compensation mode compensates for the loss of the resonant tanks. At t_4, the voltages u_{C5a} and u_{C6a} on the resonant capacitors increase to $-0.5U_{PV}$ at a linear rate, respectively. At this stage,

$$i_{La}(t) = I_L = i_{S5a} \tag{1}$$

$$u_{Ca}(t) = U_{Ca}(t_3) - \frac{I_L}{C_r}t \tag{2}$$

Here, $i_{La}(t)$ and $u_{Ca}(t)$ respectively represent general current and voltage of resonant inductors and resonant capacitors.

2) *Stage 5* [t_4, t_5]: Referring to Fig. 4(b). At t_4, the charge current of the resonant capacitors sharply decreases to zero, and the resonant inductor current is transferred into the freewheeling clamping diodes D_{a1} and D_{a2}. The inverter goes into the normal freewheeling period.

$$i_{La}(t) = I_L = i_{Da} \tag{3}$$

$$u_{Ca}(t) = -U_{Ca} \tag{4}$$

$$i_{S5a} = 0 \tag{5}$$

It is worth noting that the resonant inductors are involved in the freewheeling loop, and the currents through S_{5a} and S_{6a} are naturally dropped to zero. Thus the ZCS turn off condition for the auxiliary switches S_{5a} and S_{6a} is achieved.

3) *Stage 6* [t_5, t_6]: Referring to Fig. 4(c). At t_5, the main switches S_5 and S_6 are turned on. After that, the current in the resonant inductors decreases at a constant slope from I_L, and the current through S_5 and S_6 increases with the same slope from zero. Therefore, the ZCS turn on condition for the high frequency main switches S_5 and S_6 is achieved. The decreasing rate of the resonant inductor current is controlled by the input voltage amplitude and resonant inductance. At t_6, the current through the resonant inductors and freewheeling clamping diodes fall to zero. As a result, the reverse recovery problem is alleviated, for the ZCS turn off condition for the freewheeling clamping diodes D_{a1} and D_{a2} is naturally achieved.

$$i_{La}(t) = I_L - \frac{U_{PV}}{2L_r}t = i_{Da} \tag{6}$$

$$u_{Ca}(t) = -U_{Ca} \tag{7}$$

$$i_{S5}(t) = \frac{U_{PV}}{2L_r}t \tag{8}$$

Based on the analysis of three new modes and residual modes described in [11], no extra current is superposed on the grid current, which means the resonant action has no effect on the grid current THD.

III. Circuit Performance Analysis

A. Soft Switching Requirements

At stage 6 in *Section* II. C, the high frequency main switches S_5 and S_6 are turned on with zero current. After that, the current through S_5 and S_6 increases at a constant slope from zero, and the increasing rate of the switch current is controlled by the input voltage U_{PV} and resonant inductance L_r. The increasing rate is expressed in (8). Besides, the high frequency main switches S_5 and S_6 can be turned off with the ZCS condition at stage [t_1, t_3], and the detailed operation analysis can refer to [11]. Therefore, the SLF target for the main switches S_5 and S_6 can be realized as long as the following terms are satisfied.

$$\begin{cases} L_r > 0 \,\&\, I_{La} > I_L \\ \pi\sqrt{L_r C_r} < D_1 T_S \le T_S - \dfrac{\pi\sqrt{L_r C_r}}{2} \\ \dfrac{1}{\omega_r}\sin^{-1}\left(\dfrac{I_L}{I_{La}}\right) \le \Delta \le \pi\sqrt{L_r C_r} - \dfrac{1}{\omega_r}\sin^{-1}\left(\dfrac{I_L}{I_{La}}\right) \end{cases} \quad (9)$$

At stage [t_0, t_1] (referring to Fig. 3), the auxiliary switches S_{5a} and S_{6a} are turned on with zero current. Then the current through S_{5a} and S_{6a} increases from zero at a sine slope, and the increasing rate is expressed as bellow,

$$i_{La}(t) = I_{La}\sin[\omega_r(t-t_0)] = i_{S5a} \quad (10)$$

The auxiliary switches S_{5a} and S_{6a} can be turned off with ZCS at stage 5[t_4, t_5]. Thus, the SLF target for the auxiliary switches S_{5a} and S_{6a} can also be realized as long as the following condition is satisfied.

$$D_2 T_S \ge \pi\sqrt{L_r C_r} \quad (11)$$

In addition, the current through the freewheeling clamping diodes D_{a1} and D_{a2} decreases in a linear style from I_L to zero at stage 6 [t_5, t_6]. The decreasing rate of the diode current is controlled by the input voltage U_{PV} and resonant inductance L_r, as expressed as bellow,

$$i_{La}(t) = I_L - \frac{U_{PV}}{2L_r}t = i_{Da} \quad (12)$$

As a result, the freewheeling diodes naturally commutate and do not suffer from severe reverse recovery problem.

It is worth noting the antiparallel diodes D_1-D_4 of the line frequency switches S_1-S_4 are no longer involved in the freewheeling loop (referring to Fig. 4(c)) in the SLF-H6-I. As a result, the reverse recovery problem of the former antiparallel diodes D_1-D_4 is avoided.

It is truth that the line-frequency switches S_1-S_4 turn on and turn off with nearly a zero current in Fig. 2 (b) and their switching frequency equals the line-frequency, the line-frequency switches S_1-S_4 have an ignorable switching loss. Therefore, it can be found that the SLF-H6-I works with SLF for all semiconductor devices approximately, and a new SLF concept for transformerless PV grid-connected inverters has been realized in circuit.

B. Voltage Stresses and Loss Analysis of Power Devices

From Fig. 3, the voltage stresses of the high frequency main switches (S_5 and S_6) and the auxiliary switches (S_{5a} and S_{6a}) are the half of the input voltage. These mean that low voltage rated power devices with high performance can be employed in the high input voltage applications to reduce the conduction loss and cost. The voltage stress of the resonant capacitors C_{5a} and C_{6a} is also the half of the input voltage, which means that low voltage rated film capacitors can be used to reduce the leakage current loss and cost.

The voltage stresses of the line-frequency switches (S_1-S_4) and the freewheeling clamping diodes (D_{a1} and D_{a2}) equal the input voltage. Table I shows the quantity and voltage stress rating of power components. It can be found that the SLF-H6-I topology has approximately voltage stresses as the H6-I and ZCT-H6-I topologies.

In order to evaluate the lossless advantage of proposed SLF concept quantitatively, the semiconductor losses of several topologies have been calculated. They include the H6-I, ZCT H6-I and SLF H6-I, and the detailed data is listed in Table II. Here, the power switches used are IKW40N60T from Infineon, and the power diodes used are by RHRG5060 from Fairchild Semiconductor. They are accordant with the experiment prototype in the next section. In addition, the loss calculation process and formula have already been presented in [5] and is therefore not duplicated here.

TABLE I
COMPONENT QUANTITY AND VOLTAGE RATE IN SEVERAL TOPOLOGIES

	Voltage Rating	HS-H6-I	ZCT-H6-I	SLF-H6-I
Main switch	U_{PV}	4	4	4
	$U_{PV}/2$	2	2	2
Auxiliary switch	$2U_{PV}$	0	1	0
	U_{PV}	0	2	2
Diode	U_{PV}	4	5	2
	$U_{PV}/2$	4	6	4
Resonant component	Inductor	0	2	2
	Capacitor	0	2	2

As can be seen in Table II, the SLF-H6-I is with the least semiconductor device losses, and its switching loss and reverse recovery loss are zero. For this reason, the total semiconductor losses of the SLF-H6-I are able to be independent of the switching frequency. Therefore, the lossless advantage will be getting more outstanding as the switching frequency increases.

TABLE II
SEMICONDUCTOR LOSSES OF SEVERAL TOPOLOGIES RATED AT 50 KHZ / 1 KW

Topology	Cond. loss (W)	Switch. loss (W)	Freew. loss (W)	Rev. recov. loss (W)	Gate loss (W)	Total (W)
H6-I	11.57	12.97	4.00	11.66	0.64	40.48
ZCT-H6-I	13.22	6.03	4.00	11.66	0.96	35.87
SLF-H6-I	13.22	0	8.88	0	0.64	22.73

C. Common-Mode Characteristic

The leakage current induced by the common-mode voltage is another concern for transformerless PV grid-connected inverters. Basically, the leakage current property can be assessed by the common-mode voltage performance [32]. In brief, the leakage current of a full-bridge transformerless inverter depends on the amplitude and frequency of the common-mode voltage under the condition of filter inductor symmetric placement in phase line and neutral line.

Ignoring the switching current ripple in the output filter inductors, the differential-mode and common-mode voltages of the proposed SLF-H6-I can be listed in Table III according to the switching states. Here $u_{DM} = u_{1N} - u_{2N}$, and $u_{CM} = 0.5 \times (u_{1N} + u_{2N})$. As shown in Table III, the differential-mode voltage u_{DM} of the SLF-H6-I is an unipolar SPWM style, and the common-mode voltage u_{CM} is a constant value at all operation stages. As a result, the SLF-H6-I topology has the same differential-mode and common-voltage characteristics as the

H6-I and ZCT-H6-I topologies. Therefore, the leakage current index of the SLF-H6-I will satisfy the grid standards and codes, such as VDE 0126-1-1, IEEE 1547 *et al*..

TABLE III
SWITCH STATES, OPERATION LEVELS, DIFFERENTIAL-MODE, AND COMMON-MODE VOLTAGE OF THE SLF-H6-I

Switching Stage	u_{1N}	u_{2N}	u_{DM}	u_{CM}
$[t_0, t_3]$	U_{pv}	0	U_{pv}	$U_{pv}/2$
$[t_3, t_4]$	$U_{pv}-u_{C5a}$	u_{C6a}	$U_{pv}-2u_{Ca}$	$U_{pv}/2$
$[t_4, t_5]$	$U_{pv}/2$	$U_{pv}/2$	0	$U_{pv}/2$
$[t_5, t_9]$	U_{pv}	0	U_{pv}	$U_{pv}/2$

Note: u_{1N} is the voltage between midpoint 1 and terminal *N* in Fig. 2 (a), u_{2N} is the voltage between midpoint 2 and terminal *N*.

D. Discussion on SLF-H6-I with Non-Unity Power Factor

The aforementioned analysis is based on the assumption that the grid-connected inverter works with unity power factor, and the compact SLF-H6-I topology is derived with omitting the anti-parallel diodes of the line-frequency switches. On the other side, a definite amount of reactive power for PV grid-connected inverters has been required by the latest grid codes. For instance, German standard VDE-AR-N 4105 (updated in 2011) claims that grid-tied PV inverters of the power rating over 4.6 kVA (single phase)/13.8 kVA (three phase) should satisfy the power factor from 0.9 leading to 0.9 lagging [34]. The detail specification is shown in Table IV.

TABLE IV
DISPLACEMENT FACTOR OF THE POWER SYSTEM UNDER DIFFERENT POWER RATINGS (STD. VDE-AR-N4105)

Power Rating	Displacement Factor Requirement
PGS/PGU≤3.68 kVA	0.95(under-excited) to 0.95(over-excited) without control
3.68 kVA<PGS/PGU PGS/PGU≤13.8 kVA	0.95(under-excited) to 0.95(over-excited) commanded by power companies
PGS/PGU>13.8 kVA	0.9(under-excited) to 0.9(over-excited) commanded by power companies

PGS/PGU: power generation system/power generation unit.
The required displacement factor accuracy is 0.01.

In fact, the SLF-H6-I can also work under non-unity power factor if the anti-parallel diodes of line-frequency switches are remounted. At the same time, in order to increase the reactive power output ability, the unipolar SPWM modulation should be switched to the bipolar SPWM in out of phase of grid voltage and grid-in current. The reason is in order to supply sufficient voltage to magnetize the filter inductor. Undoubtedly, the complexity of the circuit topology and driving logic will increase. Besides, some operation regions will lose ZCS because the timing sequence of the resonant tanks is no longer satisfied for the sake of producing reactive power.

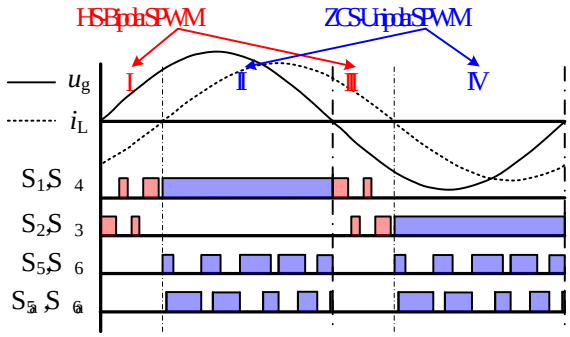

Fig. 5. Gate signals of the SLF-H6-I with lagging power factor.

The corresponding driving logic is shown in Fig. 5. Taking the grid-in current lagging grid voltage as example, when the grid-in current and grid voltage are in phase, the SLF-H6-I can still work under ZCS with unipolar SPWM; when the grid-in current reverses the grid voltage, the SLF-H6-I enters into the hard switching (HS) mode with bipolar SPWM. In addition, the reverse recovery of the anti-parallel diodes D_5 and D_6 of the high frequency main switches will cause additional loss in the HS mode. In order to reduce the loss, the fast recovery diodes can be chosen as the anti-parallel diodes of the high frequency main switches S_5 and S_6 because the anti-parallel diode of IGBT can be optimized separately. Considering the cost and reliability, the proposed topology is therefore preferred to operate at unity power factor.

Fortunately, the power rating below 3.68 kVA is still permitted to work with unity power factor only, so the proposed topology is valuable for low power applications in the future.

IV. EXPERIMENTAL RESULTS AND DISCUSSIONS

In order to verify the effectiveness of the main contributions of this paper, a 1 kW prototype with the topology shown in Fig. 2(b) is built and tested. The main components and parameters are listed as follows, U_{PV}: 360-400V DC; u_g: 180-240 V RMS/50 Hz; switching frequency f_s: 50 kHz; C_{dc1}, C_{dc2}: 470

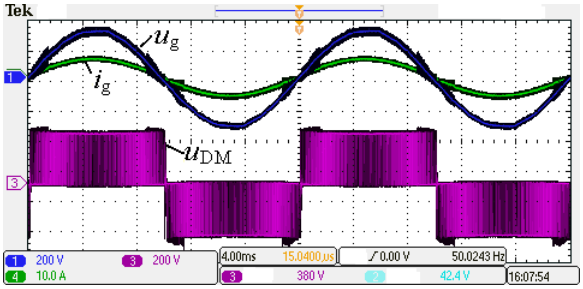

Fig. 6. Waveforms of the grid voltage u_g, the grid-in current i_g, and the differential-mode voltage u_{DM}. (u_g and u_{DM}: 200V/div, i_g: 10A/div, and time: 4ms/div).

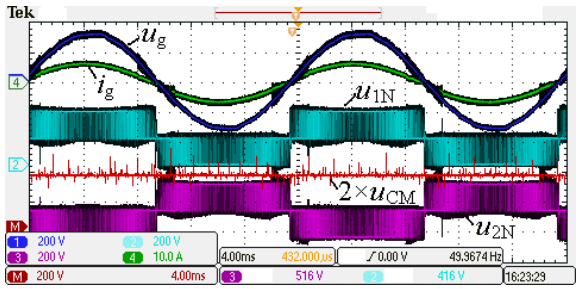

Fig. 7. Waveforms of the grid voltage u_g, the grid-in current i_g, and the common-mode voltage u_{CM}, as well as the arm voltages u_{1N} and u_{2N}. (u_g, u_{1N}, u_{2N}, and u_{CM}: 200V/div, i_g: 10A/div, and time: 4ms/div).

μF/350 V DC; L_1, L_2: 0.5 mH; C_1: 2 μF; S_1-S_6: IKW40N60T; S_{5a}, S_{6a}: IKW40N60T; D_{a1}, D_{a2}: RHRG5060.

The inductance and capacitance of the resonant tanks are the key parameters for the SLF-H6-I topology because they determine the soft switching range, maximum duty cycle, and current stress. Referring to the design guidelines and steps of the resonance parameters in [11], the key parameters L_r=23 μH and C_r=47 nF are selected and assembled. In this case, maximum I_L=6.43 A, I_{La}=8.13 A, T_r=6.28 μs, and the turn on current rise rate of the high frequency main and auxiliary switches K=8.7 A/μs.

The following experimental results are obtained at P_{out}=1 kW, u_g=230 V/50 Hz, and U_{PV}=380 V. The experimental results of the differential-mode and common-mode performance are shown in Fig. 6 and Fig. 7, respectively. It can be seen that the differential-mode voltage is an unipolar SPWM style, and the common-mode voltage is a constant value. These two factors are very important for the efficiency and leakage current performance indicators of transformerless PV grid-connected inverters. It can be found that the experimental results are in agreement with the theoretical analysis of *Section* III. C, so the SLF-H6-I topology is suitable for transformerless PV grid-connected applications [32, 33].

Fig. 8 shows the experimental waveforms of the gate driving u_{GE5}, u_{GE5a}, the resonant current i_{L5a}, and the resonant voltage u_{C5a}. As can be seen in Fig. 8, the peak voltage across the resonant capacitor is stably clamped at the half of the input voltage. It is worth noting that the processes of the start-resonating and stop-resonating of the resonant tank are safe and reliable. The experimental waveforms are in agreement with the theoretical analysis in Fig. 3.

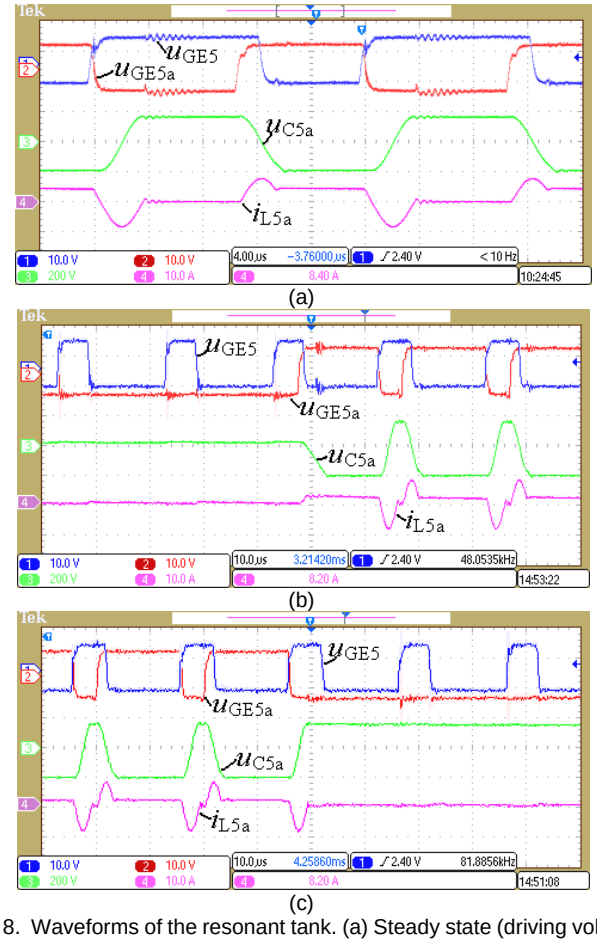

Fig. 8. Waveforms of the resonant tank. (a) Steady state (driving voltage u_{GE5} of switch S_5 and driving voltage u_{GE5a} of switch S_{5a}: 10V/div, u_{C5a}: 200V/div, i_{L5a}: 10A/div, and time: 4μs/div); (b) Start-resonant process (time: 10μs/div); (c) Stop-resonant process.

The experimental results of the ZCS of the high frequency main switches and auxiliary switches are shown in Fig. 9 and Fig. 10, respectively. It can be concluded that ZCS turn on and turn off are realized for all power IGBTs, which minimizes the switching losses. It is worth noting that the steady-state voltage stresses of the high frequency main switches and auxiliary switches are equivalent to the half of the input voltage. However, some voltage spikes can be found in the auxiliary switches voltage waveforms during the transition period, which is caused by the resonance between the resonant inductor and the parasitic capacitor of the auxiliary switch. Fortunately, the resonance energy is relatively small, and the voltage spikes are still in an acceptable range.

The experimental waveforms of the freewheeling clamping diode D_{a1} are shown in Fig. 11. It can be seen that the voltage stress of the freewheeling clamping diodes is equivalent to the

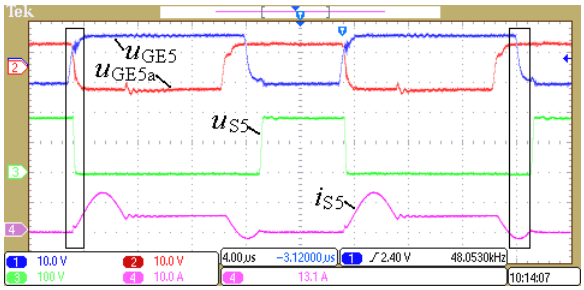

Fig. 9. Waveforms of the high frequency main switch S_5. (u_{GE5} and u_{GE5a}: 10V/div, u_{S5}: 100V/div, i_{S5}: 10A/div, and time: 4μs/div)

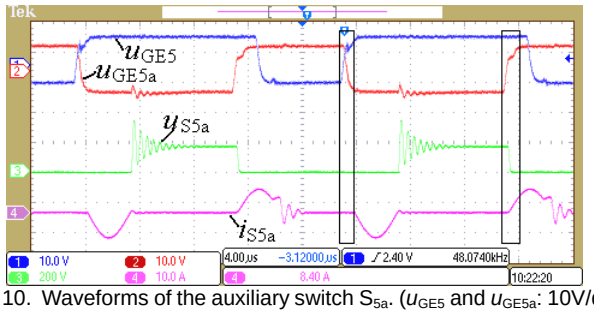

Fig. 10. Waveforms of the auxiliary switch S_{5a}. (u_{GE5} and u_{GE5a}: 10V/div, u_{S5a}: 200V/div, i_{S5a}: 10A/div, and time: 4μs/div).

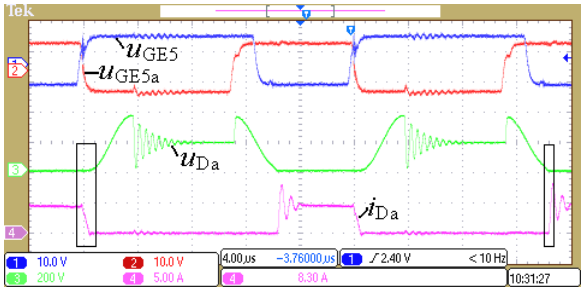

Fig. 11. Waveforms of the auxiliary diode D_{a1}. (u_{GE5} and u_{GE5a}: 10V/div, u_{Da}: 200V/div, i_{Da}: 5A/div, and time: 4μs/div).

This article has been accepted for publication in a future issue of this journal, but has not been fully edited. Content may change prior to final publication. Citation information: DOI 10.1109/TIE.2017.2694398, IEEE Transactions on Industrial Electronics

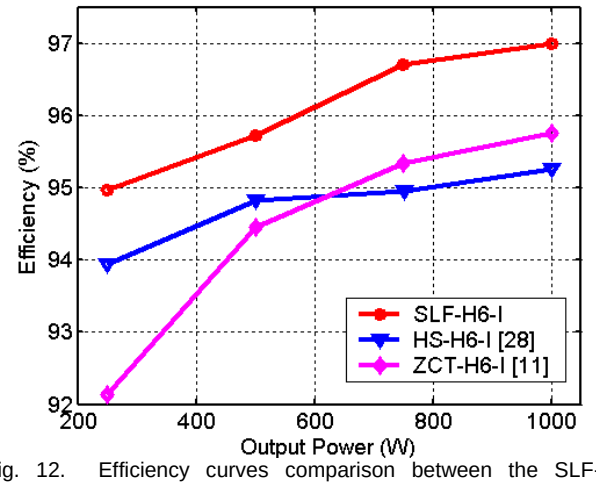

Fig. 12. Efficiency curves comparison between the SLF-H6-I, ZCT-H6-I [11], and HS-H6-I [28] (measured by Digital Power Analyzer VOLTECH PM3300).

input voltage. The current falling rate of the freewheeling clamping diodes is controlled by the resonant inductance, so the freewheeling clamping diodes are turned off naturally. As a result, the reverse recovery current of freewheeling clamping diodes is alleviated, which reduces the reverse recovery loss and the EMI noise. Considering the experimental results in Fig. 9-11, the SLF concept for the H6-I transformerless PV grid-connected inverter is realized in practice.

In order to verify the merit of the SLF concept in efficiency, the efficiency curves of the SLF-H6-I, ZCT-H6-I, and hard switching H6-I (HS-H6-I) with different output powers are shown in Fig. 12. It can be seen that the efficiency at full load is 97%, and is at least for 1.5 % improvement compared with ZCT-H6-I and HS-H6-I topologies thanks to adopting the SLF concept. More importantly, the SLF-H6-I efficiency is higher than the HS-H6-I in the full load range, which means that the sum of the increased conduction loss and resonant components loss is less than the reduced switching losses in the proposed SLF-H6-I topology.

Based on above theoretical analysis and experimental data, Table V compares and summarizes some typical hard-switching transformerless PV inverter topologies and two soft-Switching Topologies in Price and Performance aspects. As can be seen in Table V, the main disadvantage of the SLF-H6-I is in terms of passive components and diodes, which are necessary to help realize SLF. Fortunately, under the precondition of keeping same conversation efficiency, the switching frequency of the SLF-H6-I can be raised to shrink the AC filter, which is normally expensive in price. As a result, the saving cost from the AC filter can compensate for the cost of auxiliary circuit and diodes of the SLF-H6-I.

V. Conclusion

The soft-switching technique is one of the most promising techniques to raise the switching frequency for PV grid-connected inverters. The main contributions of this paper are that the SLF concept for single-phase transformerless full bridge topologies has been proposed and the SLF concept is realized based on the H6-I topology. Several clear merits are summarized as below.

1) A resonance trajectory with the self-compensation mode is designed, and a couple of the resonant tanks with the self-compensation mode are obtained based on the H6-I. They are able to compensate for the loss of the resonant tanks precisely.

TABLE V

Comparison of Hard-Switching and Soft-Switching Topologies in Price and Performance

		HERIC		H5		HS-H6-I		ZCT-H6-I		SLF-H6-I	
Input DC capacitors	Quantity(piece)	1		1		2		2		2	
	Voltage	U_{PV}		U_{PV}		$U_{PV}/2$		$U_{PV}/2$		$U_{PV}/2$	
	Price	High		High		Low		Low		Low	
Switches	Quantity(piece)	4(HF[1])	2(LF[2])	3(HF)	2(LF)	2(HF)	4(LF)	4(HF)	4(LF)	4(HF)	4(LF)
	Voltage	U_{PV}	U_{PV}	U_{PV}	U_{PV}	$U_{PV}/2$	U_{PV}	$U_{PV}/2$	U_{PV}	$U_{PV}/2$	U_{PV}
	Price	High	Medium	High	Medium	Medium	Medium	High	Medium	Medium[3]	Medium
Diodes	Quantity	0		0		2		1	2	2	
	Voltage					$U_{PV}/2$		$2U_{PV}$	$U_{PV}/2$	U_{PV}	
	Price	None		None		Low		Medium	Low	Low	
Passive components	Quantity (set)	1(AC[4])		1(AC)		1(AC)		1(AC)	2(Aux[5])	1(AC)	2(Aux)
	Voltage/Current	U_{PV}/I_{Lp}[6]		U_{PV}/I_{Lp}		U_{PV}/I_{Lp}		U_{PV}/I_{Lp}	$U_{PV}/2\ /I_{La}$[7]	U_{PV}/I_{Lp}	$U_{PV}/2\ /I_{La}$
	Price	High		High		High		High	Very low	High	Very low
Losses	Switching	High		High		High		Medium		Almost zero	
	Conduction	Low		Medium		High		High		High	
	Total	Medium		High		High		Medium		Low	
Heat-Sink (Volume/Price)		Medium		High		High		Medium		Low	
EMI noise		High		High		High		Medium		Low	
Leakage current		Medium		Medium		Medium		Low		Low	
Reactive power ability		Good		Good		Good		Not recommend		Not recommend	

[1]: HF means high frequency operation;
[2]: LF means line frequency operation;
[3]: can choose low speed switches because of no switching losses;
[4]: AC means output filter at AC side, which composes of inductor and filter;
[5]: Aux means resonant components in the resonant tank, which composes of inductor and filter;
[6]: I_{Lp} represents the maximum amplitude of the grid-in current;
[7]: I_{La} represents the maximum amplitude of the resonant current.

2) The ZCS conditions are achieved for all power switches in both of turn on and turn off processes under unity power factor condition. Besides, the ZCS turn off of the freewheeling diodes is achieved naturally so that the reverse recovery problem is alleviated.

3) By integrating the resonant tank and clamping diodes with saving one diode, the freewheeling clamping function is obtained synchronously so that a constant common-mode voltage is realized at switching frequency scale.

These characteristics are verified by a SLF-H6-I prototype rated at 50 kHz, 1 kW. In brief, the proposed SLF concept is a good candidate for the high frequency transformerless PV inverters, especially in the unity power factor application below 4.6 kW rated power.

REFERENCES

[1] W. Li, Y. Gu, H. Luo, W. Cui, X. He, and C. Xia, "Topology review and derivation methodology of single-phase transformerless photovoltaic inverters for leakage current suppression," *IEEE Trans. Ind. Electron.*, vol. 62, DOI 10.1109/TIE.2015.2399278, no. 7, pp. 4537-4551, July, 2015.

[2] T. Yi, Y. Wenli, L. Poh Chiang, and F. Blaabjerg, "Highly reliable transformerless photovoltaic inverters with leakage current and pulsating power elimination," *IEEE Trans. Ind. Electron.*, vol. 63, DOI 10.1109/TIE.2015.2477802, no. 2, pp. 1016-1026, Feb. 2016.

[3] T. K. S. Freddy, N. A. Rahim, W. P. Hew, and H. S. Che, "Modulation techniques to reduce leakage current in three-phase transformerless H7 photovoltaic inverter," *IEEE Trans. Ind. Electron.*, vol. 62, DOI 10.1109/TIE.2014.2327585, no. 1, pp. 322-331, Jan. 2015.

[4] H.. Xiao, K. Lan, and L. Zhang, "A quasi-unipolar SPWM full-bridge transformerless PV grid-connected inverter with constant common-mode voltage," *IEEE Trans. Power Electron.*, vol. 30, DOI 10.1109/TPEL.2014.2331367, no. 6, pp. 3122–3132, Jun. 2015.

[5] H. Xiao, S. Xie, C. Yang, and R. Huang, "An optimized transformerless photovoltaic grid-connected inverter," *IEEE Trans Ind. Electron.*, vol. 58, DOI 10.1109/TIE.2010.2054056, no. 5, pp. 1887-189, May, 2011.

[6] L. Zhang, K. Sun, Y. Xing, and M. Xing, "H6 transformerless full-bridge PV grid-tied inverters," *IEEE Trans. Power Electron.*, vol. 29, DOI 10.1109/TPEL.2013.2260178, no. 3, pp. 1229-1238, Mar. 2014.

[7] Y. Gu, W. Li, Y. Zhao, B. Yang, C. Li, and X. He, "Transformerless inverter with virtual DC bus concept for cost-effective grid-connected PV power systems," *IEEE Trans. Power Electron.*, vol. 28, DOI 10.1109/TPEL.2012.2203612, no.24, pp. 793-805, Feb. 2013.

[8] H. Xiao, and S. Xie, "Transformerless split-inductor neutral point clamped three-level PV grid-connected inverter," *IEEE Trans. Power Electron.*, vol. 58, DOI 10.1109/TPEL.2011.2164940, no. 1, pp. 184-191, Jan. 2011.

[9] B. Gu, J. Dominic, J.-S. Lai, C.-L. Chen, T. LaBella, and B. Chen, "High reliability and efficiency single-phase transformerless inverter for grid-connected photovoltaic systems," *IEEE Trans. Power Electron.*, vol. 28, DOI 10.1109/TPEL.2012.2214237, no. 5, pp. 2235-2245, May 2013.

[10] E. Koutroulis and F. Blaabjerg,, "Design optimization of transformerless grid-connected PV inverters including reliability," *IEEE Trans. Power Electron.*, vol. 28, DOI 10.1109/TPEL.2012.2198670, no. 1, pp. 325-335, Jan. 2013.

[11] H. Xiao, K. Lan, B. Zhou, L. Zhang, and Z. Wu, "A Family of Zero-Current-Transition Transformerless Photovoltaic Grid-Connected Inverter," *IEEE Trans. Power Electronics*, vol. 30, DOI 10.1109/TPEL.2014.2337513, no. 6, pp. 3156~3165, Jun. 2015.

[12] H. Xiao, X. Liu, and K. Lan, "Zero-Voltage-Transition Full-Bridge Topologies for Transformerless Photovoltaic Grid-Connected Inverter," *IEEE Trans Ind. Electron.*, vol. 61, DOI 10.1109/TIE.2014.2300044, no. 10, pp. 5393-5401, Oct. 2014.

[13] V. Gupta, S. Khajehoddin, P. Jain, "Phase-staggered multiple ZVS inverters for grid-connected PV systems," in *Proc. IEEE ECCE*, vol. 1, DOI 10.1109/ECCE.2013.6647303, Sept. 2013, pp. 4503-4510.

[14] C. Du, X. Zhang, and D. Xu, "Study on an active clamping soft switching grid-connected inverter," in *Proc. IEEE APEC*, vol. 1 DOI 10.1109/APEC.2012.6165825, Feb. 2012, pp. 232-239.

[15] R. Li, Z. Ma, and D. Xu, "A novel active clamping zero-voltage switching Grid-connected three-phase inverter," in *Proc. IEEE ECCE*, vol. 1, DOI 10.1109/ECCE.2010.5618280, Sept. 2010, pp. 2164-2171.

[16] Y. Zhao, T. Wei, H. Hu, and Y. Xing, "A high-efficiency PV grid-tied micro-inverter with soft switching for dc/ac stage," in *Proc. IEEE ICIEA*, vol. 1, DOI 10.1109/ICIEA.2015.7334280, June 2015, pp. 1150-1154.

[17] D. Amorndechaphon, "High-efficiency PWM DC-AC inverter for small PV power generation system," in *Proc. IEEE ICUE*, vol. 1, DOI 10.1109/COGEN.2016.7728941, Sept. 2016, pp. 1-6.

[18] K. R. Sree, A. K. Rathore, E. Breaz, and F. Gao, "Soft-switching non-isolated current-fed inverter for PV/fuel cell applications," *IEEE Trans Ind. Appl.*, vol. 52, DOI 10.1109/TIA.2015.2472360, no. 1, pp. 351-359, Jan. 2016.

[19] D. Divan, "The resonant dc-link converter- a new concept in power conversion," *IEEE Trans Ind. Appl.*, vol. 25, DOI 10.1109/28.25548, no. 2, pp. 317-325, Mar/Apr. 1989.

[20] O. In-Hwan and Y. Myung-Joong, "A simple soft-switched PWM inverter using source voltage clamped resonant circuit," *IEEE Trans Ind. Electron.*, vol. 46, DOI 10.1109/41.753787, no. 2, pp. 468-471, Apr. 1999.

[21] S. Mandrek and P. Chrzan, "Quasi-resonant DC-link inverter with a reduced number of active elements," *IEEE Trans Ind. Electron.*, vol. 54, DOI 10.1109/TIE.2007.895143, no. 4, pp. 2088-2094, Aug. 2007.

[22] Y. Gu, L. Hang, S. Chen, Y. Du, Z. Lu, and Z. Qian, "Research on control type soft switching converters," in *Proc. IEEE PESC*, vol. 1, DOI 10.1109/PESC.2004.1355641, June 2004, pp. 1470-1475.

[23] S. Gong, M. Yang, X. Ding, and B. He, "Research of interleaved three-phase bidirectional DC/DC converter based on control type soft switching", in *Proc. IEEE ICEMS*, vol. 1, Oct. 2008, pp. 1738-1741.

[24] G. Koo, G. Moon, M. Youn, "New zero-voltage-switching phase-shift full-bridge converter with low conduction losses," *IEEE Trans. Ind. Electron.*, vol. 52, DOI 10.1109/TIE.2004.841063, no. 1, pp. 228-235, Feb. 2005.

[25] M. Arias, D. Lamar, F. Linera, D. Balocco, A. Diallo, and J. Sebastian, "Design of a soft-switching asymmetrical half-bridge converter as second stage of an LED driver for street lighting application," *IEEE Trans. Power Electron.*, vol. 27, DOI 10.1109/TPEL.2011.2164942, no. 3, pp. 1608-1621, March, 2012.

[26] L. Hang, S. Wang, Y. Gu, W. Yao, Z. Lu, "High cross-regulation multioutput series resonant converter with magamp postregulator," *IEEE Trans. Ind. Electron.*, vol. 58, DOI 10.1109/TIE.2010.2098374, no. 9, pp. 3905-3913, Sep. 2011.

[27] M. Bellar, T. Wu, A. Tchamdjou, J. Mahdavi, and M. Ehsani, "A review of soft-switched dc–ac converters," *IEEE Trans. Ind. Appl.*, vol. 34, DOI 10.1109/28.703992, no. 4, pp. 847–860, Jul./Aug. 1998.

[28] G. Hua, and F. Lee, "Soft-switching techniques in PWM converters," *IEEE Trans. Ind. Electron.*, vol. 42, DOI 10.1109/41.475500, no. 6, pp. 595-603, Dec. 1995.

[29] G. Hua, C. Leu, Y. Jiang, and F. Lee, "Novel zero-voltage-transition PWM converters," *IEEE Trans. Power Electron.*, vol. 9, DOI 10.1109/63.286814, no. 2, pp. 213-219,March, 1994.

[30] G. Hua, E. Yang, Y. Jiang, and F. Lee, "Novel zero-current-transition PWM converters," *IEEE Trans. Power Electron.*, vol. 9, DOI 10.1109/63.334775, no. 6, pp. 601-606, Nov. 1994.

[31] R. Gonzalez, J. Lopez, P. Sanchis, and L. Marroyo, "Transformerless inverter for single-phase photovoltaic systems," *IEEE Trans. Power Electron.*, vol. 22, DOI 10.1109/TPEL.2007.892120, no. 2, pp. 693–697, Mar. 2007.

[32] H. Xiao, and S. Xie, "Leakage current analytical model and application in single-phase transformerless photovoltaic grid-connected inverter," *IEEE Trans. Electromag. Comp.*, vol. 52, DOI 10.1109/TEMC.2010.2064169, no. 4, pp. 902-913, Nov., 2010.

[33] X. Guo, and X. Jia, "Hardware-based cascaded topology and modulation strategy with leakage current reduction for transformerless PV systems," *IEEE Trans. Ind. Electron.*, vol. 62, DOI 10.1109/TIE.2016.2607163, no. 12, pp. 7823–7832, Dec. 2016.

[34] "VDE-AR-N 4105:2011-08 Power generation systems connected to the low-voltage distribution network, " VDE Association for Electrical, Electronic and Information Technologies, Frankfurt, 2011.

Hua F. Xiao (S'10–M'13) was born in Hubei Province, China. He received the B.S., M. S. and Ph.D. degrees in electrical engineering from Nanjing University of Aeronautics and Astronautics, Nanjing, China, in 2004, 2007 and 2010, respectively.

He joined the Faculty of power electronics in 2011, and is currently an Associate Professor at the College of Electrical Engineering, Southeast University, Nanjing, China. From 2015 to 2016, he was a Postdoctoral Fellow with the Department of Electrical and Computer Engineering, Ryerson University, Toronto, ON, Canada. From Aug. 2016, he is a Postdoctoral Fellow with the Department of Electrical and Computer Engineering, McGill University, Montreal, QC, Canada.

Dr. Xiao's research interests include high frequency soft-switching conversions, photovoltaic power systems, and applications of power electronic technology in power system. Dr. Xiao has authored more over 40 technical papers in Journals and Conference proceedings, and held 13 china patents.

Li Zhang was born in Anhui, China, in 1990. He received the B.S. degree in 2012 from Tianjin Polytechnic University, and is currently working towards the M.S. degree in electrical engineering in Southeast University, Nanjing, China.

His current research interest includes photovoltaic grid-connected inverters.

Yanqing Li was born in Jiangsu, China, in 1993. He received the B.S. degree in 2012 from Huaiyin Institute of Technology, and is currently working towards the M.S. degree in electrical engineering in Southeast University, Nanjing, China.

His current research interest includes new energy development and utilization technology.